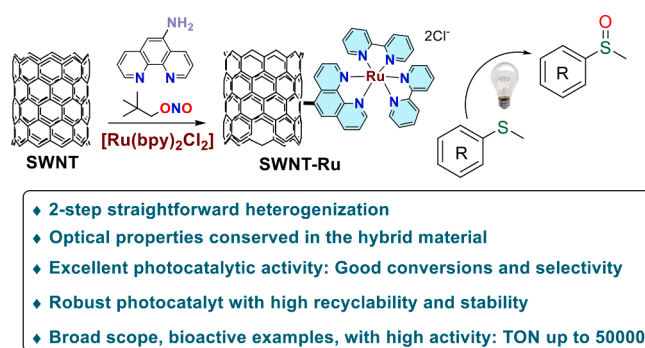


Regular Article

Single walled carbon nanotubes covalently functionalized by a ruthenium complex for photocatalytic oxidations

Paula Blanco-Caamano^a, Cristina Navío^b, Matías Blanco^{a,c,*}, José Aleman^{a,c,d,*}^a Organic Chemistry Department, Universidad Autónoma de Madrid, 28049 Madrid, Spain^b IMDEA Nanociencia, Ciudad Universitaria de Cantoblanco, c/Faraday 9, 28049 Madrid, Spain^c Institute for Advanced Research in Chemical Sciences (IAdChem), Universidad Autónoma de Madrid, 28049 Madrid, Spain^d Center for Innovation in Advanced Chemistry (ORFEO-CINQA), Universidad Autónoma de Madrid, Madrid 28049, Spain

GRAPHICAL ABSTRACT



ARTICLE INFO

Keywords:

Carbon nanotubes
Functionalization
Ruthenium complexes
Photochemistry
Oxidation

ABSTRACT

The covalent bonding of a ruthenium bipyridine complex derivative with the aromatic network of single walled carbon nanotubes (SWNT) through a stepwise protocol is presented, thus yielding the sample **SWNT-Ru**. To do that, an-amino decorated phenanthroline is bonded to the nanotube by means of the diazonium chemistry protocol, providing anchoring points for discrete organometallic units as depicted by the solid characterization techniques employed. The hybrid material, able to emit upon excitation, is active in the visible light-driven photocatalytic oxidation of organic sulfides to sulfoxides. **SWNT-Ru** presents a wide scope being able to convert more than 10 substrates with different characteristics, including added-value chemicals, with a stable performance over more than 6 cycles without metal leaching and enhanced activity compared to related homogeneous complexes. A versatile character is also demonstrated since this hybrid catalyst follows both possible photooxidation mechanisms.

* Corresponding authors at: Organic Chemistry Department, Universidad Autónoma de Madrid, 28049 Madrid, Spain.

E-mail addresses: matias.blanco@uam.es (M. Blanco), jose.aleman@uam.es (J. Aleman).

<https://doi.org/10.1016/j.jcis.2024.05.018>

Received 12 February 2024; Received in revised form 29 April 2024; Accepted 4 May 2024

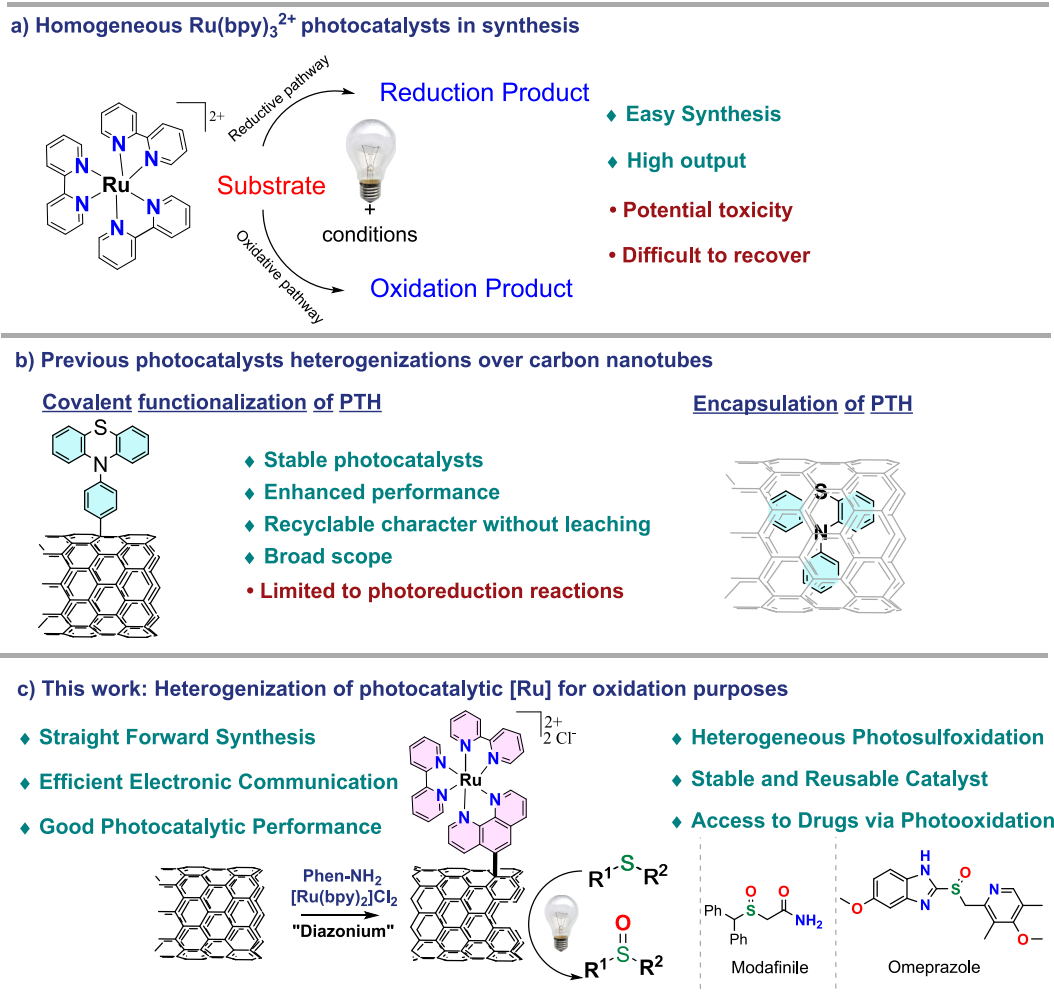
Available online 5 May 2024

0021-9797/© 2024 The Author(s). Published by Elsevier Inc. This is an open access article under the CC BY-NC-ND license (<http://creativecommons.org/licenses/by-nc-nd/4.0/>).

1. Introduction

Artificial photosynthetic systems able to harvest sunlight energy and convert it into chemical vectors that yield organic molecules suppose an inspiring but still challenging task [1]. Indeed, light-driven organic reactions have gathered nowadays several attention in order to transform classic systems onto easier-to-manage and more sustainable synthetic pathways for fine chemicals, fuels, commodities or drugs manufacturing among other examples [2]. Under these premises, photoredox catalysis reaches new reactivities otherwise impossible under classic methodologies [3], being the mild conditions employed and light as energy source able to trigger chemical phenomena the main characteristics [4]. One of the most popular, efficient and active photoredox systems relies on the $\text{Ru}(\text{bpy})_3^{2+}$ (bpy = 2,2'-bipyridine) family of complexes (Scheme 1a) [5]. They catalyze a vast bunch of organic reactions, such as cycloadditions, radical additions, reductive dehalogenations, the cleave of protecting groups by reductive or oxidative mechanisms and they oxidize functional groups too [6]. In particular, the chemoselective oxidation of sulfides to sulfoxides has become an important transformation useful, for example, in the preparation of drugs (such as modafinile or omeprazole, Scheme 1c) but also ligands and key intermediates in organic synthesis [7–9]. Hence, photoredox catalysis develops methodologies that avoid hazardous oxidants as peroxides or peracids (such as *m*-chloroperbenzoic acid), yielding the target sulfoxide products [10]. Under photoredox conditions, a wide gamut of sulfoxides commodities of different nature may be easily prepared.

Nevertheless, the limited activity that photoredox catalysts usually present, combined with the often-slow reaction rate due to active species lifetimes, charge separation, high cost and potential hazard metal contamination may hamper further applicability of this catalytic field [6,11]. Aiming to solve these common problems, researchers looked for adequate supports to heterogenize the (photo)active species (Scheme 1b), and by rational design [12], generating a hybrid material that synergistically works towards the target product [13]. In this way, some examples have been reported with the employment of carbon nanomaterials as carbon nanotubes and graphene as support of homogeneous photoredox catalysts [14]. The heterogenization has been done by different methods, such as direct mixing (whose stability is usually compromised) [15], by elaborated synthetic protocols to modify both nanocarbon and photoactive species and set a covalent bond [16], by a direct link between partners (both electrostatic or covalent) [17,18], by sequential sidewall construction (specially for organometallic units) or by encapsulation in the inner cavity of the carbon nanotubes [19,20]. Most of these examples relied on the heterogenization of photocatalysts with a strong reductive character. Besides the additional stability and easy of recovery to the photoactive unit due to the heterogenization [21], carbon nanomaterials are able to increase the reaction rate by enhancing the charge separation through photoelectron injection or hole replenishing thanks to the inherent conductivity [22]. The surface chemistry has been reported to take a role in the catalytic cycle [17], and the porous carbon structure combined with their aromatic nature could furnish reactants to the active centers by local surface concentration



Scheme 1. a) the potential of $\text{Ru}(\text{bpy})_3^{2+}$ as photocatalyst; b) previous heterogenizations of reductive photocatalysts on carbon nanotubes compared to c) this work based on the heterogenization of a related $\text{Ru}(\text{bpy})$ complex for the target photooxidation.

phenomena [23]. Nevertheless, the number of reports where a Ru(bpy)₃²⁺ or related photoactive complexes have been heterogenized in nanocarbon supports, is still very scarce, in particular for oxidative processes that would lead to the obtaining of drugs and commodities presented above. Currently, the Ru(bpy)₃²⁺ has been successfully heterogenized in porous organic and metal–organic frameworks [24–26], at the surface of inorganic semiconductors [27–29], in silicas [30–32], in polymers [33], or in graphene-related materials with results comparable to the homogeneous run besides providing photostability [34]. However, to the best of our knowledge this powerful photocatalytic unit has never been covalently immobilized on carbon nanotubes before, even some non-covalent decoration for photophysical studies have been reported [35]. Thus, a robust covalent bond would be desirable for expanding beyond the state-of-the-art the applicability of this family of SWNT-catalysts and provide a solution to the typical homogeneous chemistry problems (Scheme 1c).

Therefore, in this work we present the stepwise sidewall construction of a Ru(bpy)₃²⁺ related complex via direct and controlled heterogenization of a chelating phenanthroline unit through the diazonium chemistry protocol and further complexation. As a result, discrete organometallic units of 1.3 nm of diameter (matching the size of the complex) were observed covalently bonded to the surface of single walled carbon nanotubes (SWNT), with a degree of functionalization as high as 3.6 wt%. The hybrid material was tested as catalyst in a visible-light chemoselective photoredox oxidation of sulfides to sulfoxides, outperforming homogeneous complexes, and accomplishing the reaction in a wide variety of substrates, presenting extending recyclability and stability towards operation. The catalyst operated through both possible mechanisms and was able to synthesize added-value chemicals such as omeprazole and modafinile.

2. Experimental

2.1. General Information, materials and methods

All chemicals, solvents and reagents, including single walled carbon nanotubes (SWNT, Aldrich), were purchased from commercial sources (reagent grade quality or better) and used without further purification if not otherwise stated. Purification of organic products, when necessary, was accomplished by flash chromatography using silica gel (Merck Geduran® Si 60) in an adequate mixture of cyclohexane (CyH) and ethyl acetate (EtOAc) eluents. All the organic products were characterized by comparison of their ¹H NMR spectral data with those reported in the literature or from commercial sources. The synthesis of ruthenium complexes **1** and **2** are fully described in the Supporting Information (S. I.).

Nuclear Magnetic Resonance (NMR) spectra were acquired on a BRUKER AVANCE spectrometer running at 300 MHz for ¹H and are internally referenced to the residual CDCl₃ signal: δ 7.26 ppm for ¹H NMR. Data for ¹H NMR are reported as follows: chemical shift (δ ppm), multiplicity, coupling constant *J* (Hz) and integration. Transmission Electron Microscopy (TEM) images were acquired with a JEOL-JEM 2100F instrument equipped with a CCD high resolution camera and an Oxford EDX spectrometer *in situ* microprobe. Samples were drop casted from 0.5 mg mL⁻¹ nanotube methanol suspensions on holey-carbon copper grids. For the elemental analysis measurements, a LECO CHNS-932 Analyser (Model NO: 601–800-500) was used. Total X-Ray Fluorescence analysis (TXRF) were performed with a benchtop S2 PicoFox TXRF spectrometer from Bruker Nano (Germany). TXRF system was equipped with a Mo X-ray source working at 50 kV and 600 μ A, a multilayer monochromator with 80 % of reflectivity at 17.5 keV (Mo K α), a XFlash SDD detector with an effective area of 30 mm² and an energy resolution better than 150 eV for 5.9 keV (Mn K α) [19]. For deconvolution and integration, commercial Spectra v.7.5.3 software package from Bruker was used. X-Ray Photoemission Spectroscopy (XPS) measurements were performed under Ultra High Vacuum

conditions (UHV, with a base pressure of 5×10^{-10} mbar), using a monochromatic Al K α line as exciting photon source for core level analysis ($h\nu = 1486.7$ eV). The emitted photoelectrons were collected in a hemispherical energy analyser (SPHERA-U7, pass energy set to 20 eV for the XPS measurements to have a resolution of 0.6 eV) and to compensate the built-up charge on the sample surface it was necessary the use of a Flood Gun (FG-500, Specs), with low energy electrons of 3 eV and 40 μ A. C 1s sp² centred at 284.4 eV is taken as binding energy reference. Samples were stack on high purity carbon scotch tape on a Mo holder and left outgas overnight in high vacuum prior to the measurements. Thermogravimetric analysis (TGA) measurements were carried out with a thermobalance TGA Q500 from TA Instruments with a ramp of 10 °C min⁻¹ under a nitrogen atmosphere from 100 to 1000 °C. The Raman spectra were collected using a Witec alpha300 R Raman microscope using a laser with an excitation wavelength of 532 nm (0.1 mW), focused on the sample with a 100x objective. The maps were collected over the regions of interest by selecting a square area and further pixel adjusting to 1 μ m². Then, the area was scanned with a rate of 0.5 s integration time over each pixel. The presented spectra are the mean over all the data acquired. The map construction represents a balance of the regions where the peak at 1595 cm⁻¹ (G band) is maximized against the regions where the peak at 1340 cm⁻¹ (D band) is maximized. UV–Vis absorption spectra were collected at a Cary 50 spectrometer (Varian), in the 200–800 nm range. In this case, TEM suspensions were employed for solid samples, while molecules were naturally dissolved. Emission spectra were recorded using an Edinburg Instruments FS5 Spectrofluorometer. HPLC grade MeOH solvent and a 10x10 mm light path quartz SUPRASIL® cuvette equipped with a silicone/PTFE septum were used for all measurements. Emission spectra of the light sources used for the photochemical reactions were recorded on an optical spectrometer StellarNet model Blue-Wave UV-NB50 (see Figure S1 at S.I.). The reactor consisted of a custom-made temperature-controlled system, where the reaction mixture was kept at room temperature by passing coolant through the metallic system employing a recirculating chiller, and the irradiation was achieved with a single LED (21 mW green LED at 520 nm, 22 mW blue LED at 450 nm, 18 mW purple LED at 420 nm, 40 mW white LED, for more details see S.I.) located 1 cm beneath the base of the vial.

2.2. Nanotubes functionalization. Synthesis of SWNT-Phen and SWNT-Ru

Firstly, commercially available SWNT (50 mg) were purified by treatment with concentrated hydrochloric acid through magnetically stirring at 60 °C for 2 h [36]. The etched solid was cleaned by centrifugation with fresh Milli-Q water with the necessary centrifugation cycles till the supernatant reached neutral pH. After drying under vacuum, the procedure yielded the sample purified SWNT. 24 mg of those SWNT (ca. 2 mmol of carbon) was added in a round bottom flask with 0.15 mmol (0.029 mg) of 5-amino-1,10-phenanthroline, and then suspended in 20 mL of acetonitrile [37]. Finally, 0.5 mmol (0.058 mL) of *tert*-butyl nitrite was added. The reaction was magnetically stirred at room temperature for 16 h. Then, the reaction mixture was washed by centrifugation, the supernatant was discarded and the black powder was collected, suspended in 15 mL of *N,N*-dimethylformamide (DMF), sonicated during 1 min, and centrifuged again. This washing procedure was repeated with DMF (4 x 15 mL), methanol (MeOH) (3 x 15 mL), aqueous HCl 1 M (2 x 15 mL), water (3 x 15 mL), methanol (2 x 15 mL), and finally with acetone (2 x 20 mL). Drying under vacuum afforded the corresponding SWNT-Phen sample. For the synthesis of sample SWNT-Ru [38], 12 mg of SWNT-Phen was suspended in 10 mL of EtOH under inert atmosphere, to where 0.04 mmol (0.02 g) of [Ru(bpy)₂Cl₂] (bpy = bipyridine) was added. The reaction was magnetically stirred at 80 °C for 3 days, and then the mixture was filtered through a 0.45 μ m polytetrafluoroethylene (PTFE) membrane. The black powder was collected, suspended in 20 mL of fresh ethanol, sonicated for 1 min and filtered

again. This procedure was repeated 4 times, and 2 additional times using acetone as washing solvent. Drying under vacuum afforded sample **SWNT-Ru**.

2.3. Catalysis, recovery and leaching

A typical catalytic reaction, if not otherwise stated, was performed as follows: A vial was charged with a magnetic stirring bar, the organic substrate **3a-j** (0.1 mmol), the catalyst (1 mg for nanotubes-based materials, 5 mol% for complexes **1** or **2**) and solvent (1 mL). The vial was sealed and irradiated with a 450 nm LED at 20 °C using a reactor that includes a thermostatic jacket where the coolant is pumped through by a chiller at constant temperature (see inset in [figure S1](#) at S.I.). Thus, the reaction was set for the desired time, typically 6 h. A 0.05–0.1 mL aliquot was withdrawn at regular intervals and analyzed by NMR spectroscopy to monitor the progress of the reaction. The reaction under O₂ was set by bubbling with pure O₂ for 10 min before sealing the vial. Yields, unless otherwise stated, were determined by isolation of the product by extracting the organic molecules from the reaction with 15 mL of dichloromethane 3 times, combination of organic layers, drying with MgSO₄, concentration and flash chromatography (silica, CyH – EtOAc) if necessary [39].

The recovery and recycling experiments were performed as follows: Sample **SWNT-Ru** was recovered by filtration over a PTFE membrane and washed with 3 cycles of DMF, 3 cycles of MeOH, 1 cycle of H₂O, 3 cycles of MeOH and 3 cycles of acetone, sonicating for 1 min between each cycle. Then, sample was vacuum-dried. After that, the heterogeneous catalyst was set for a new photo-oxidation of sulfide **3a** with 1 mL of water. The reaction nevertheless was allowed to proceed for 5 h under 450 nm illumination (~70 % conversion), and the crude was analyzed by NMR spectroscopy. This procedure was repeated 5 times. In the case of the homogeneous photocatalyst, endurance tests were performed by adding fresh amount of **3a** (0.1 mmol) to the vial after reaction completion for several additional reaction cycles. Furthermore, a hot-filtration configuration was adopted to evaluate eventual ruthenium leaching. Thus, substrate **3a** was photooxidized under standard conditions, and when the reaction reached 30 % and 70 % conversion, the catalyst was filtered out from the reaction, the filtrate was returned to the LED allowing the reaction to proceed. Aliquots were withdrawn to monitor the reaction progress, while TXRF analysis was done to the reaction liquids. Finally, mechanistic studies were conducted under standard conditions but adding various amounts of the selected quencher, *i.e.*, sodium azide, 9,10-dimethylanthracene or 1,4-dimethoxybenzene, to the reaction mixture [39].

3. Results

3.1. Synthesis and characterization

Commercial single walled carbon nanotubes (SWNT) of 0.9 nm diameter and several μ m in length were employed in all the experiments. However, they were subjected to a wet acid treatment aiming the removal of carbonaceous impurities as well as metals responsible of the nanotubes' growth [36], yielding purified **SWNT**. After this impurity etch, the nanotubes were observed very clean, with a smooth carbon structure, (see TEM picture below and [Supporting Information](#), S.I.) while any significant content of metals was neither observed by TEM nor detected by the TXRF analysis of this sample (see S.I.). However, the acid etching modified the chemical composition, showing an oxygen content of 19 wt%. (see elemental analysis, [Table 1](#)). On the other hand, homogeneous Ru complexes were prepared for comparative purposes. In particular, we prepared Ru(bpy)₂(phen)Cl₂ **1** and Ru(bpy)₂(phen-NH₂)Cl₂ **2** (phen = 1,10-phenanthroline; phen-NH₂ = 5-amino-1,10-phenanthroline) following a procedure described previously in the literature [40,41], and the obtained spectroscopy data of complexes **1** and **2** totally matched the reported data (see S.I. for synthesis and

Table 1

Elemental analysis, Raman and TXRF data.

Sample	C ^a	H ^a	N ^a	S ^a	I _D /I _G	Ru ^b
SWNT	77.5	1.8	0.4	0.1	0.05	–
SWNT-Phen	72.5	2.4	2.1	0.5	0.17	–
SWNT-Ru	74.5	2.5	3.1	0.1	0.18	3.6

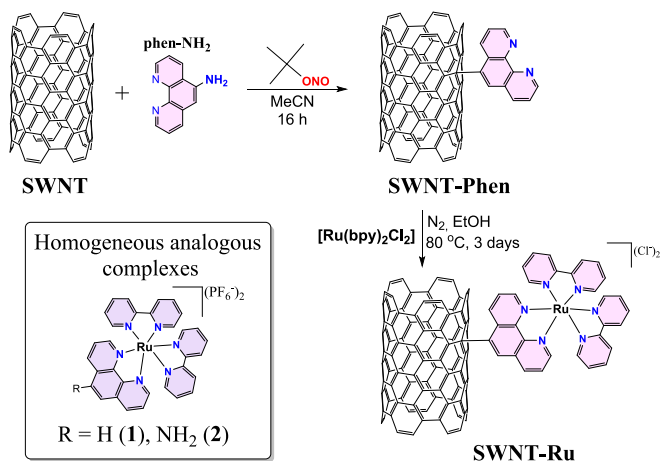
a) Elemental analysis determination, values given in wt.%; b) TXRF determination, value given in wt.%.

characterization details).

The heterogenization of the Ru complex was planned by a stepwise sidewall functionalization of the carbon structure of purified **SWNT** sample, according to [scheme 2](#). Briefly, **SWNT**, **phen-NH₂** and neopentyl nitrite were mixed to *in situ* generate a diazonium salt able to extrude nitrogen and then react with the walls of the nanotube, yielding the sample **SWNT-Phen** where the phenanthroline is covalently attached to the surface of the nanotubes, following an adapted procedure of the literature [37,38]. A further derivatization by chelation of [Ru(bpy)₂Cl₂] with this sample was undertaken under hot conditions to promote the coordination of the metal to the anchoring point of the bonded phenanthroline, which yielded sample **SWNT-Ru**.

The functionalization of the carbon nanotubes was tracked by different solids characterization techniques. On the one hand, the elemental analysis of the samples detected an increase in the N content (see [Table 1](#)). For instance, purified **SWNT** sample presented a low 0.4 wt% content of N, which was increased up to 2.1 wt% of N for sample **SWNT-Phen** as a result of the introduction of the phenanthrolines at the side wall of the nanotubes. In addition, the complexation of the Ru(bpy)₂ unit resulted in a further increase in the N content, which reached 3.2 wt% as a consequence of the additional N atoms present at the bipyridines ligands. Interestingly, the ruthenium analysis by TXRF of sample **SWNT-Ru** afforded 3.6 wt% (see S.I. for further details), which totally matches the N determination elucidated from the elemental analysis considering that each complex carries 6 N atoms. TGA crosschecked the results (see S.I.), since a 13 % weight loss was detected below 400 °C for sample **SWNT-Phen** and 22 % weight loss for sample **SWNT-Ru** (totally matching the elemental analysis determination), accompanied by a higher residue (30 % vs 10 % for the non-metalated sample) after the heating, which could indicate that the remaining metal content may come from the introduced ruthenium complex [42].

On the other hand, Raman spectroscopy was employed to analyze the extent and homogeneity of the functionalization treatment ([Fig. 1](#)). From the Raman spectrum of purified sample **SWNT**, the radial breathing mode (RBM) at 200–300 cm⁻¹ of Raman Shift, the defect band (D band) associated to the vibration of C sp³ bonds at 1343 cm⁻¹ and the



Scheme 2. Functionalization of carbon nanotubes, including the structure of homogeneous analogous references **1** and **2**.

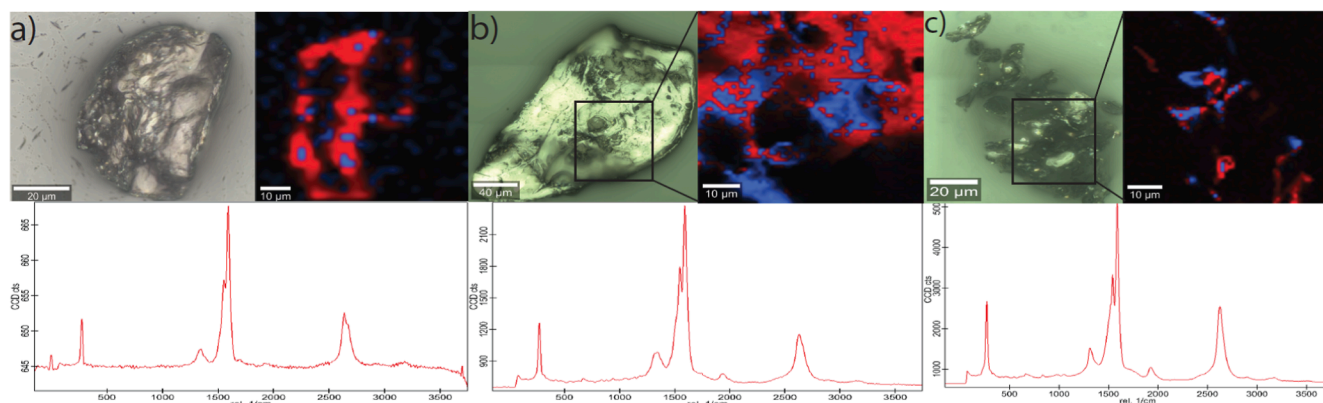


Fig. 1. Optical image, Raman map and mean Raman spectrum of samples: a) SWNT, b) SWNT-Phen and c) SWNT-Ru.

in-plane C sp² associated vibration signal (G band) at around 1595 cm⁻¹ clearly came across as the typical Raman features of single walled carbon nanotubes [43]. Since the functionalization is designed to occur at the outer surface of the nanotubes using the carbon scaffold as reactant, the nanotubes' structure is expected to be affected and more defects should be recorded in the functionalized samples. Indeed, the Raman structural parameter I_D/I_G of purified sample SWNT was calculated as 0.05, which was increased to 0.17 for the functionalized sample SWNT-Phen, while the RBM band was observed at the same position, suggesting that the hypothesis of external functionalization was correct [18,44]. In addition, similar value of I_D/I_G = 0.18 was recorded for sample SWNT-Ru, indicating that the carbon nanotube did not take part in the complexation reaction (or it was not affected by the complexation), and the Ru(bpy)₂ core only interacted with the bonded phenanthroline units. It is worthy to mention that the position of the G band of both functionalized samples SWNT-Phen and SWNT-Ru was shifted 5 cm⁻¹ to the blue (Figure S4 at S.I.), indicating a nanotube doping effect as a plausible charge transfer from the complex to the tube might take place. This effect may be a consequence of the conjugation with electron rich moieties that are able to inject charge due to resonance and

inductive effects, which is in accordance with previous report studying electron donating units directly linked to the wall of carbon nanotubes able to inject charge to the material [18]. Finally, the functionalization is a homogeneous chemical process distributed throughout the whole nanotube local aggregation, according to Raman mapping. To do that, we selected a nanotube aggregation, and we scanned the particle detecting the defective regions, denoted with blue pixels and are characteristic of the functionalization (regions where the D band is maximized) and the graphitic regions, that are labelled with red pixels (regions where the G band is maximized) [18]. It can be seen that pristine SWNT appeared mainly as a red particle in the mixed image of the Raman map, and the blue and defective regions increased in the mapping of SWNT-Phen, where those regions appeared randomly distributed over the whole area. Finally, the on-plane regions of sample SWNT-Ru reflected similar colour mixing compared to SWNT-Phen, in sharp agreement with the mean spectrum values discussed above.

The morphological characteristics of the samples were studied by HRTEM. As introduced above, a very clean and smooth surface was observed for purified sample SWNT (Fig. 2a and supporting information). The purification treatment removes all the impurities, making the

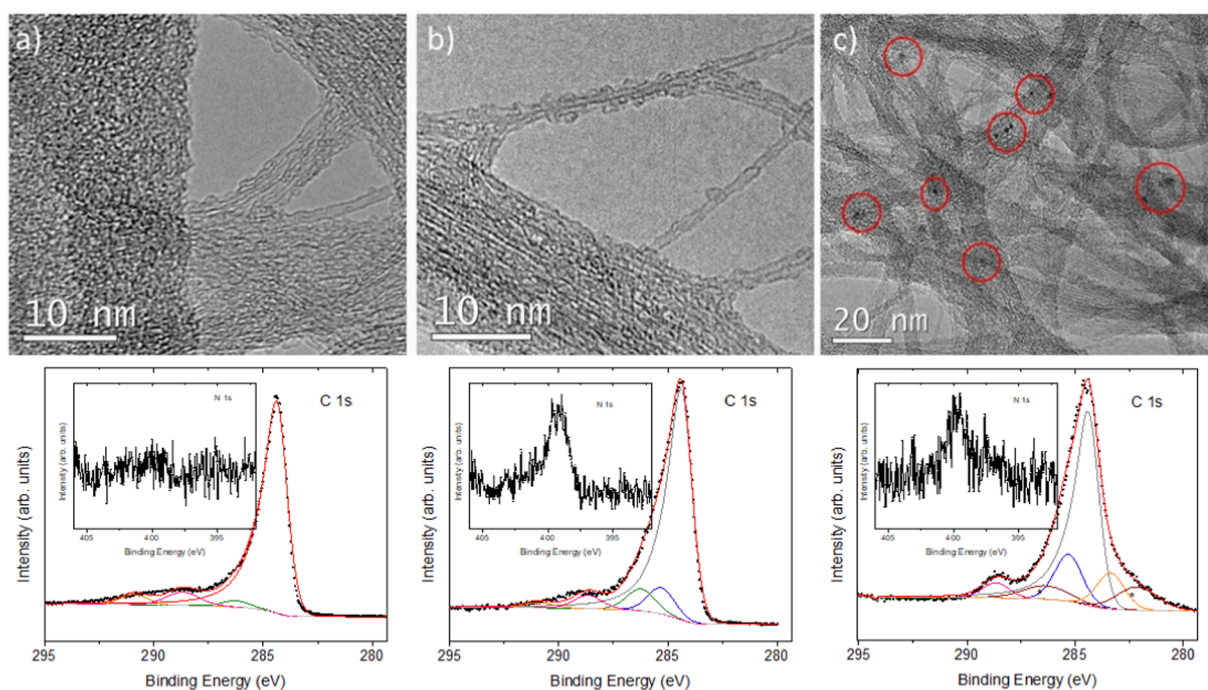


Fig. 2. HRTEM images at the upper panels of a) SWNT, b) SWNT-Phen and c) SWNT-Ru (red circles highlight the electrondense regions), accompanied at the lower panels by the corresponding C 1s and N 1s (in the inset) XPS core level regions.

tubes to appear heavily aggregated in bundles or arrays, where any other particle or protrusion could be observed. Indeed, the local EDX analysis could only detect C, besides the metal elements composing the TEM grid. After the functionalization, some organic material could be observed surrounding the nanotubes of sample **SWNT-Phen** (Fig. 2b), presenting a rougher aspect compared to the pristine and purified starting sample. The *in situ* EDX analysis performed on this sample only detected N as new element compared to the features detected for pristine sample **SWNT** (see S.I.), therefore indicating that this extra morphology could correspond to the bonded phenanthrolines. Interestingly, sample **SWNT-Ru** presented a different shape, since electrondense regions can be clearly distinguished amid the nanotube arrays (Fig. 2c). These regions accounted a mean diameter of 1.3 nm [45,46], and they were spotted in a fashion that correspond to the degree of functionalization discussed above. In addition, the *in situ* EDX analysis registered the presence of both Ru and Cl (Figures S7-S9 at S.I.). XPS analysis complemented the observed features (Fig. 2 lower panels). On the one hand, the analysis of the C 1s XPS core level region spotted that the chemical structure of pristine **SWNT** corresponded to a great majority of C sp^2 bonds, with very low amount of defective C sp^3 functions and even lower quantity of oxygenated species. In addition, the N 1s XPS core level region showed a plane region since this sample has not followed any chemical treatment besides the purification. Conversely, sample **SWNT-Phen** presented a broader C 1s spectrum, and new components merged out from the fit, being very representative the peak at 286.3 eV of binding energy (BE), which can be assigned as the C–N bonds present in the phenanthroline covalently bonded to the nanotube [47]. These bonds were also

observed at the N 1s XPS core level region, which presented a signal centered at 399.4 eV of BE in agreement with the presence of the N-containing molecule at the surface of the nanotubes. Finally, the XPS analysis of sample **SWNT-Ru** resulted in a more complicated spectrum due to the overlapping of C 1s and Ru 3d photoelectron lines. Nevertheless, a component at 281.9 eV of BE corresponding to the Ru 3d_{5/2} could be observed. The position of the BE is higher than the typical position of Ru²⁺ species and that BE reported for an anchored Ru complex on carbon nanotubes (Ru(*p*-cymene)Cl₂NH-Nanotube was reported at 281.6 eV of BE) [19,48], but the presence of 6 electronegative N atoms bonding the Ru could displace to even higher BE the chemical shift of this metal. For the same reasons, a component at 397 eV of BE was observed in the N 1s XPS core level region, as a result of the bonding of the N to the Ru atoms, thus highlighting a successful coordination.

The optical features of the heterogeneous and homogeneous samples were also analyzed by means of MeOH stable suspensions and liquid UV–Vis absorption and emission spectroscopies. On the one side, complexes **1** and **2** exhibited the reported optical features for this kind of organometallic dyes typically reported previously. In particular, both samples presented a strong absorption set of bands in the UV region corresponding to the characteristic metal centered *d-d* and ligand-centered $\pi-\pi^*$ transitions (Fig. 3a), which are strongly different between **1** and **2** due the presence of the terminal amino group, while the characteristic visible absorption bands compressing metal-to-ligand transitions are centered at 450 nm and 458 nm, respectively [49]. On the other hand, the carbon nanotube based samples presented different optical behavior. Pristine and purified **SWNT** owns the typical planar

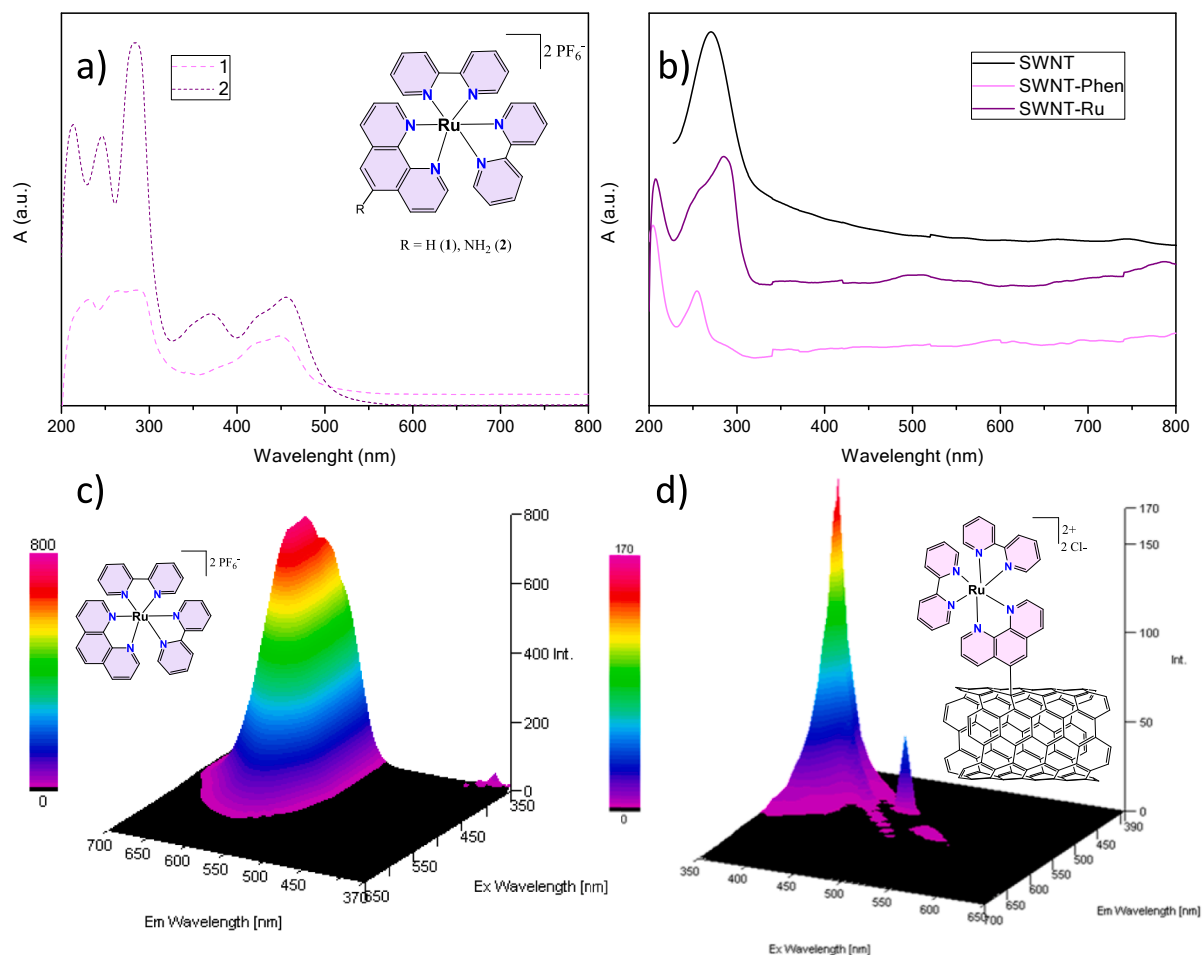


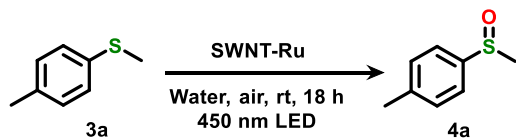
Fig. 3. UV–Vis spectroscopy data. Upper panels represent absorption spectra of a) homogeneous and b) heterogeneous sample; lower panels represent emission maps of c) sample **1** and d) sample **SWNT-Ru**.

absorption spectrum despite the scattering (Fig. 3b), with an absorption maximum centered at 270 nm as a consequence of the aromatic region [50]. Functionalized sample **SWNT-Phen** presented a very similar UV–Vis absorption spectrum, but the maximum is shifted 16 nm to the blue, in agreement with the Raman data as a result of charge injection from the electron rich phenanthroline to the carbon nanotube as discussed above [23]. Conversely, the spectrum of **SWNT-Ru** is different compared to the other materials. The aromatic band appeared at similar position, but it becomes mixed with the UV absorption band of the complex. In addition, the typical metal-to-ligand absorption band of the complex is also spotted, but it is redshifted to 490 nm, which is a symptom of a covalent functionalization according to previous reports [51]. The emission spectra were also recorded, and they were plotted as a photoluminescent (PL) map using the excitation wavelength as reference. While complexes **1** and **2** presented the typical homogeneous emission map reported for these samples (Fig. 3c and SI), the absorption features of the Ru-containing nanotube resembled the absorption spectrum (Fig. 3d), with an emission peak centered at 550 nm that would be taken in benefit for photocatalytic purposes (emission map of sample **SWNT-Phen** was also recorded and it is presented in the S.I.). As a whole, the sum of all the gathered characterization data, combined with the photocatalytic character (see below), suggests that the Ru complex has been introduced as discrete organometallic units at the surface of the nanotube using the step-wise functionalization protocol discussed.

3.2. Catalytic activity

The photocatalytic activity of the Ru-based hybrid materials was tested in the visible light photochemical oxidation of organic sulfides to the corresponding sulfoxides and compared to the homogeneous references **1** and **2** due to favorable potential alignment in order to carry out the reaction. Thus, we adopted as model reaction the oxidation of *p*-tolyl-methyl sulfide **3a** in water, under an air atmosphere and using as illumination source at 450 nm LED (see Table 2). With this set of conditions, 1 mg of **SWNT-Ru** as catalyst was able to fully promote the oxidation of the sulfide to the sulfoxide without detecting any appreciable trace of superoxidized sulfone or any other byproducts.

Table 2
Model photooxidation of sulfides studied under catalysis of **SWNT-Ru**.



Entry	Variation	Conversion (%) ^a
1	No variation	>99
2	Catalyst = 1 (5 mol%)	70 ^b
3	Catalyst = 2 (5 mol%)	44 ^b
4	Catalyst = SWNT-Phen	n.r.
5	Catalyst = SWNT	n.r.
6	No catalyst	n.r.
7	No light	n.r.
8	LED = 420 nm	41
9	LED = 520 nm	64
10	LED = white	>99
11	Solvent = MeOH	80
12	Solvent = 2-PrOH	79
13	Solvent = MeOH/H ₂ O 1:1	>99
14	Solvent = DMF	30
15	Solvent = DCM	21
16	Inert atmosphere	12

Reaction conditions: substrate **3a** (0.1 mmol), 1 mg of heterogeneous catalyst in water (1 mL) under an air atmosphere was irradiated under 450 nm light for 18 h at rt. The homogeneous **1** and **2** loading was 5 mol%. ^aConversion (%) determined by ¹H NMR; n.r. stands for no reaction. ^bSulfone was detected.

Conversely, catalysts **1** and **2** struggled to achieve this level of conversion under the same set of conditions even with a high catalyst loading of 5 mol%, since both catalysts were not able to finish the reaction in an overnight run. Indeed, catalyst **1** achieved a 70 % conversion while catalyst **2** did not reach this activity value and only accounted 44 % conversion, and in both reactions, the corresponding sulfone was detected in 5 and 21 % conversion respectively (Table 2 entries 2 and 3). Thus, the behavior of the hybrid material **SWNT-Ru** in this photocatalytic reaction clearly overcomes the catalytic parameters that homogeneous reactions resemble in terms of activity and selectivity, especially considering the high conversion achieved without adding any other additives in a reaction carried out in water. Logically, the lack of photocatalytic unit in both precursors **SWNT** and **SWNT-Phen** make them to not present activity (Table 2 entries 4 and 5). More control experiments, including the absence of catalyst or light, afforded negligible conversion. Therefore, all these experiments emphasize the very good photocatalytic behavior of sample **SWNT-Ru** in the photooxidation of organic sulfides under environmentally friendly conditions in water, which was even able to achieve conversion with other illumination sources (Table 2 entries 8–10), including green light (520 nm LED, 69 % conversion) thanks to the absorption and emission of the sample as characterized above. Blank experiments were conducted at these wavelengths too (see table S5 at S. I. for further details). While white LED afford 24 % conversion, the other wavelength showed negligible conversion. Therefore, this further optimization made as to select 450 nm LED as illumination source. Considering the amount of the ruthenium complex present in that mg of sample according to TXRF determinations, and taking into account that the catalytic activity observed is only caused by the anchored active units, **SWNT-Ru** exhibits an outstanding TON = 50000 value for this particular photocatalytic oxidation. Other typical solvents for this transformation, such as methanol, 1:1 mixture methanol–water, dichloromethane, *N,N*-dimethylformamide or isopropanol were also screened (0–80 % conversion, Table 2 entries 11–15), but the best result was achieved with water. Finally, molecular oxygen was concluded to be the oxidant of this reaction (Table 2 entry 16) since a test performed under inert atmosphere resulted in a very poor 12 % conversion.

With the optimized conditions, we analyzed the kinetics of the reaction catalyzed by the Ru-based complex by withdrawing aliquots at regular intervals and analyzing them by ¹H NMR (see Fig. 4a). As previously depicted in Table 2, the best catalyst was the hybrid material **SWNT-Ru**. This material presented sigmoidal kinetic profile similar to other heterogeneous SWNT-based catalysts reported previously [18,20,39], with a very pronounced increase in the achieved conversion after 5 h of reaction, and almost finishing the oxidation in 6 h (Fig. 4a). Conversely, samples **1** and **2** presented a *pseudo*-first order kinetics curve and started the reaction without any induction period, but after 6 h of reaction, sample **1** only reached 51 % of conversion, that was increased to the 70 % after 18 h, while sample **2** presented just 31 % of conversion in 6 h and 44 % in 18 h. The kinetics study agrees with the overnight experiments. However, analyzing the kinetics under a pure oxygen atmosphere showed a *pseudo*-first order kinetic profile for sample **SWNT-Ru** in the photooxidation of **3a** too (Figure S16 at S.I.), achieving full conversion in very similar times (8 h). This observation may indicate that the diffusion step of a key reagent as O₂ has an important role in the catalytic performance. Nevertheless, the same level of activity made us decide to select air as standard atmosphere. As a whole, all the data support the fact that the heterogenization leads to the obtaining of an excellent photocatalyst with enhanced performance. Indeed, sample **SWNT-Ru** presented a comparable or even better photocatalytic performance compared to other state-of-the-art catalysts (see benchmark table S6 at S.I.).

Over these kinetic studies, the stability of the hybrid material was evaluated. Firstly, we performed the recovery of the catalyst by filtration methods, we profusely washed to eliminate any remaining contaminant and we set a further reaction without adding any new catalyst precursor.

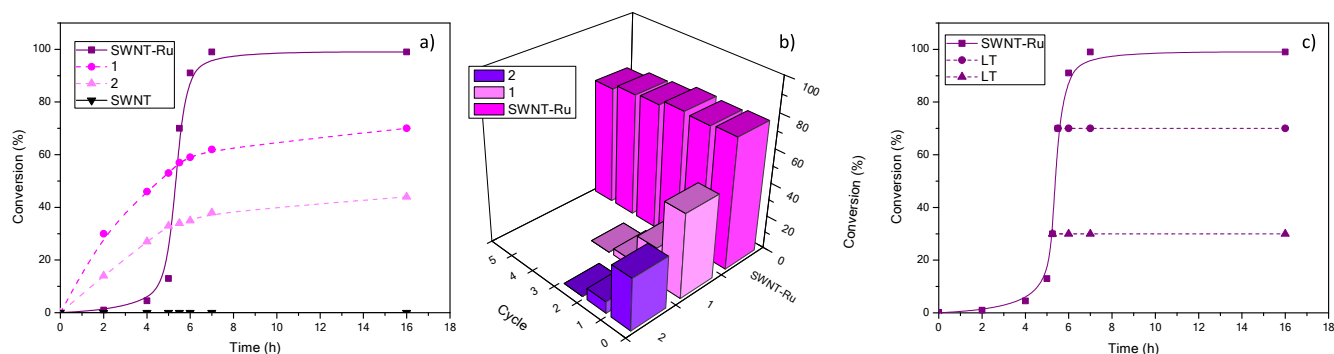
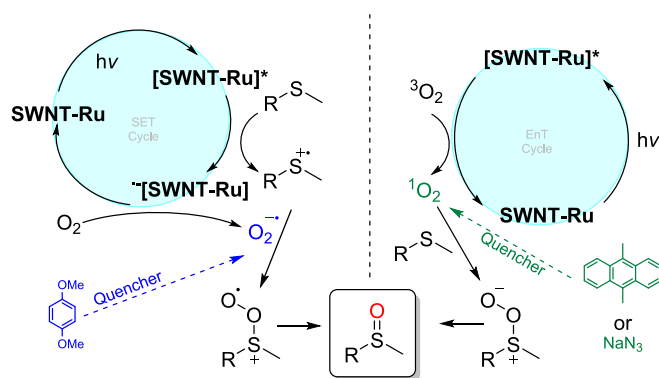


Fig. 4. a) kinetic profiles on the photooxidation of **3a** catalyzed by the different materials; b) recycling study of **SWNT-Ru** after 5.5 h of **3a** photooxidation and c) “hot filtration” experiment with **SWNT-Ru**.

We let the reaction run for 5 h and we evaluated the conversion. The procedure was repeated for 5 times, and just a tiny loss of conversion was observed for 5 consecutive runs, passing from 77 % to 72 %, maybe due to loss of catalytic material instead of catalyst deactivation (Fig. 4b). Then, two filtration experiments at around 30 % and 70 % conversion were adopted by filtering the catalyst **SWNT-Ru** out of the reaction liquids and letting the reaction to proceed for additional 11 h under illumination. Monitoring this filtrate by NMR showed any increase in the conversion of the sulfide **3a** to the sulfoxide **4a** (Fig. 4c) at both filtration points, indicating that there are not active species leached out from the nanotube able to catalyze the reaction. Indeed, TXRF analysis of the reaction waters after this “hot filtration” did not detect any trace of Ru (see S.I.), while similar 1.4 nm wide electron-dense regions were observed in the HRTEM analysis of the recovered sample, with the same catalyst loading quantified by TXRF (see S.I.) and similar $I_D/I_G = 0.18$ Raman ratio (see S.I.), demonstrating sample **SWNT-Ru** is a robust photocatalyst because, even after the recycling study, the Ru complexes supported on the carbon nanotubes are stable during operation.

The mechanism of the photooxidation performed by sample **SWNT-Ru** was analyzed by means of quenching experiments. According to the reported data, two different reaction routes are possible for the photooxidation of sulfides using air as oxidant. On the one hand, the formation of oxygen radical anion species via single electron transfer and, on the other hand, the formation of singlet oxygen as a result of an energy transfer process [52]. In order to elucidate this mechanism, the addition of quenchers was performed. Indeed, 1,4-dimethoxybenzene and sodium azide are known scavengers for electron transfer and energy transfer processes, respectively, while 9,10-dimethylantracene is known to quench singlet oxygen too [53]. Therefore, we compared the conversion value obtained for a standard run using **SWNT-Ru** as catalyst with the experiments adding the quencher (see table S7 at S.I.). The model reaction, as depicted before, afforded more than 99 % conversion after 6 h, but the conversion resulted negligible when each quencher was added to the reaction mixture in high amount (0.5 equiv.). Conversely, some conversion was observed when reducing the amount of quencher. For instance, the reaction with 1,4-dimethoxybenzene as scavenger resulted in 30 % conversion when using 0.1 and 0.25 equiv. of quencher. On the contrary, the conversion was found 15 % with 0.25 equiv. of sodium azide and 61 % with 0.1 equiv. Similar results were spotted when decreasing the amount of 9,10-dimethylantracene (60 % at 0.25 equiv. and 77 % conversion with 0.1 equiv.). These experiments indicated that **SWNT-Ru** is able to catalyze the photooxidation of sulfides by both mechanisms, thus highlighting the versatility of our hybrid photocatalyst, but the single electron transfer reaction pathway seemed more plausible. As a whole, the quenching experiments allowed us to propose the photooxidation mechanism depicted in Scheme 3.

We analyzed too the scope of the catalyst changing the characteristics of the sulfides by introducing different functional groups or substituting the aromatic ring by alkyl chains. The results are shown in



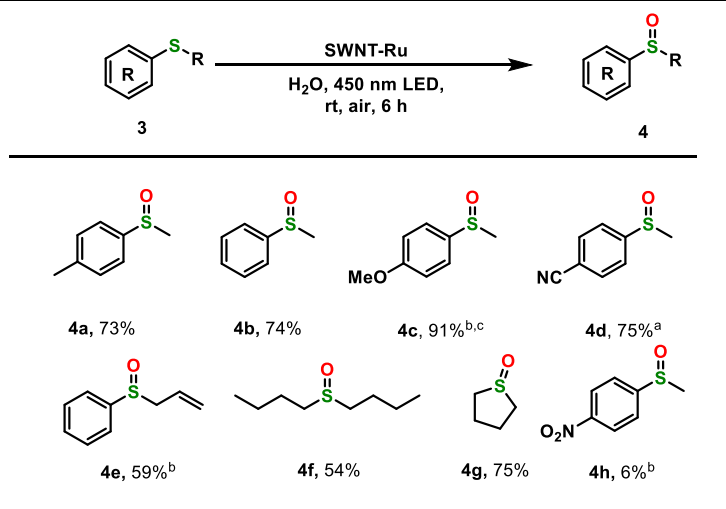
Scheme 3. Proposed mechanisms for the photooxidation of sulfides by **SWNT-Ru**.

Table 3. Indeed, the oxidation of sulfide **3a** afforded sulfoxide **4a** in 73 % yield, while the performance was maintained performing the oxidation of phenyl-methyl sulfide **3b** (74 % yield). We also added and removed electron density to the sulfur atom by placing electron donor (methoxy, **3c**) and electron withdrawing (nitrile, **3d**) groups in the corresponding *para* position. For our delight, catalyst **SWNT-Ru** straightforward performed the oxidation in both electron-modified substrates, achieving **4c** and **4d** in 91 % and 75 % yields respectively. In addition, a more challenging substrate to oxidize, *p*-nitrophenyl methyl sulfide [54], was oxidized in low yield. Furthermore, reactive groups as an allyl system were tolerated, and the substrate **4e** was obtained in a remarkable 59 % yield. Alkyl substrates can be converted too, and the catalyst **SWNT-Ru** accomplished the oxidation of both linear and cyclic dibutylsulfide **3f** and tetrahydrothiophene **3g** in 54 % and 75 % yields respectively. It is important to mention that, even some of the products needed to be purified, on each reaction crude we could not detect any trace of sulfone, denoting again the high chemoselectivity of our hybrid catalyst.

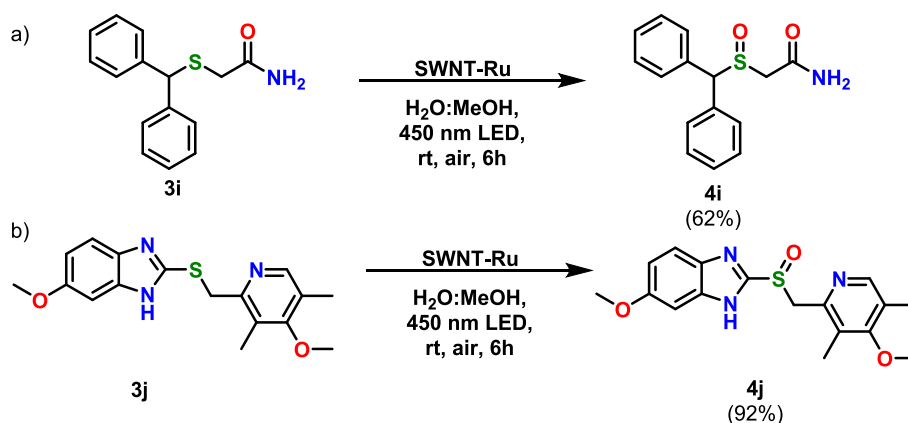
As a figure of merit, it is important to demonstrate the applicability of our hybrid material in the synthesis of relevant sulfoxides that possess demonstrated bioactivity. In this sense, we attempted the synthesis of modafinile and omeprazole, two important drugs available in common markets that content the sulfoxide group [55,56]. Selected substrates **3i** and **3j** were set to the corresponding photooxidation under standard conditions using an equimolar mixture of MeOH:H₂O as solvent to enhance the solubility of the molecules (Scheme 4). For our delight, the reaction with **3i** as substrate obtained a good 62 % yield, which is similar to the linear aliphatic substrates as depicted in Table 3. Moreover, the synthesis of enriched sulfoxide present in the omeprazole molecule **4j** was accomplished in a meritorious 92 % yield.

Table 3

Scope of the photooxidation of sulfides catalyzed by SWNT-Ru.



Reaction Conditions: substrate **3** (0.1 mmol) and 1 mg of SWNT-Ru in water (1 mL) under an air atmosphere was irradiated under 450 nm LED for 6 h at rt. Values stand for isolated yield. a) In 1:1 mixture of H₂O/MeOH. b) ¹H NMR yield determined using CH₃NO₂ as internal standard. c) 0.2 mmol scale.



Scheme 4. Synthesis of relevant bioactive added-value chemical by photocatalytic oxidation performed with SWNT-Ru. Reaction Conditions: substrate **3i-j** (0.1 mmol) and 1 mg of SWNT-Ru in 1:1 mixture water/MeOH (1 mL) under an air atmosphere was irradiated under 450 nm light for 6 h at rt. Values stand for isolated yield.

4. Conclusions

This work describes the sidewall functionalization of SWNT with a photoactive Ru organometallic complex through the diazonium chemistry and further complexation, yielding the sample SWNT-Ru. As a result of this straightforward two-steps protocol, a strong covalent immobilization of 1.3 nm discrete organometallic light-sensitive moieties was provided. Indeed, the hybrid material accounted a functionalization degree of 3.6 wt% of Ru(II) according TXRF and XPS determinations. In addition, the hybrid system was found sensitive to light able to emit in the blue region upon absorption of visible light. Therefore, this particular nanotube-based platform was employed as photocatalyst in the selective oxidation of organic sulfides to their corresponding sulfoxides. SWNT-Ru was found a competitive catalyst for this transformation, presenting a comparable or even better catalytic character than related systems for this transformation and outperforming homogeneous references. It was able to complete the photooxidation in 6 h, owing a TON = 50000 with a recyclable character able to prevent metal leaching. In addition, SWNT-Ru demonstrated to be a versatile photocatalyst, performing the oxidation of a variety of

substrates, including bioactive added-value chemicals through the two plausible mechanisms of this transformation. We believe that adding an organometallic-SWNT hybrid resource for expanding the possibilities in photoredox catalysis, especially in a heterogeneous approach, will be very beneficial for the community.

CRediT authorship contribution statement

Paula Blanco-Caamano: Validation, Methodology, Investigation. **Cristina Navío:** Formal analysis, Data curation. **Matías Blanco:** Writing – review & editing, Writing – original draft, Methodology, Investigation, Conceptualization. **José Aleman:** Writing – review & editing, Supervision, Conceptualization.

Declaration of competing interest

The authors declare the following financial interests/personal relationships which may be considered as potential competing interests: Jose Aleman reports financial support, administrative support, and article publishing charges were provided by Autonomous University of

Madrid. Jose Aleman reports a relationship with Autonomous University of Madrid that includes: employment. If there are other authors, they declare that they have no known competing financial interests or personal relationships that could have appeared to influence the work reported in this paper.

Data availability

No data was used for the research described in the article.

Acknowledgments

This work was supported by MICINN (PID2021-122299NB-I00, TED2021-129999B-C32, TED2021-130470B-I00), VIRMAT Projects in response to COVID-19 financed by the ERDF-REACT-EU resources, “Comunidad de Madrid” for European Structural Funds (S2018/NMT-4367) and proyectos sinérgicos I + D (Y2020/NMT-6469).

Appendix A. Supplementary data

Supplementary data to this article can be found online at <https://doi.org/10.1016/j.jcis.2024.05.018>.

References

- [1] S. Berardi, S. Drouet, L. Francàs, C. Gimbert-Suriñach, M. Guttentag, C. Richmond, T. Stoll, A. Llobet, Molecular artificial photosynthesis, *Chem. Soc. Rev.* 43 (2014) 7501–7519.
- [2] X.-Y. Yu, J.-R. Chen, W.-J. Xiao, Visible light-driven radical-mediated C-C Bond cleavage/functionalization in organic synthesis, *Chem. Rev.* 121 (2021) 506–561.
- [3] N.E.S. Tay, D. Lehnher, T. Rovis, Photons or electrons? a critical comparison of electrochemistry and photoredox catalysis for organic synthesis, *Chem. Rev.* 122 (2022) 2847.
- [4] N. Hoffmann, Photochemical reactions as key steps in organic synthesis, *Chem. Rev.* 108 (2008) 1052–1103.
- [5] C.P. Anderson, D.J. Salmon, T.J. Meyer, R.C. Young, Photochemical generation of Ru(bpy)₃³⁺ and O₂·, *J. Am. Chem. Soc.* 99 (1977) 1980–1982.
- [6] C.K. Prier, D.A. Rankic, D.W.C. MacMillan, Visible light photoredox catalysis with transition metal complexes: applications in organic synthesis, *Chem. Rev.* 113 (2013) 5322–5363.
- [7] E. Skolia, P.L. Gkizis, C.G. Kokotos, A sustainable photochemical aerobic sulfide oxidation: access to sulforaphane and modafinil, *Org. Biomol. Chem.* 20 (2022) 5836–5844.
- [8] E. Skolia, P.L. Gkizis, C.G. Kokotos, Aerobic Photocatalysis: Oxidation of Sulfides to Sulfoxides, *ChemPlusChem* 87 (2022) e202200008.
- [9] B.M. Trost, M. Rao, Development of chiral sulfoxide ligands for asymmetric catalysis, *Angew. Chem. Int. Ed.* 54 (2015) 5026–5043.
- [10] X. Zhang, K.P. Rakesh, L. Ravindar, H.-L. Qin, Visible-light initiated aerobic oxidations: a critical review, *Green Chem.* 20 (2018) 4790–4833.
- [11] R. Ahmad, Z. Ahmad, A.U. Khan, N.R. Mastoi, M. Aslam, J. Kim, Photocatalytic systems as an advanced environmental remediation: Recent developments, limitations and new avenues for applications, *J. Environ. Chem. Eng.* 4 (2016) 4143–4164.
- [12] C.H. Mak, X. Han, M. Du, J.-J. Kai, K.F. Tsang, G. Jia, K.-C. Cheng, H.-H. Shen, H.-Y. Hsu, Heterogenization of homogeneous photocatalysts utilizing synthetic and natural support materials, *J. Mater. Chem. A* 9 (2021) 4454–4504.
- [13] N. Waiskopf, Y. Ben-Shahar, U. Banin, Photocatalytic hybrid semiconductor-metal nanoparticles; from synergistic properties to emerging applications, *Adv. Mater.* 30 (2018) 1706697.
- [14] S. Fukuzumi, Y.-M. Lee, W. Nam, Immobilization of molecular catalysts for enhanced redox catalysis, *ChemCatChem* 10 (2018) 1686–1702.
- [15] T.B. Ogunbayo, T. Nyokong, Phototransformation of 4-nitrophenol using Pd phthalocyanines supported on single walled carbon nanotubes, *J. Mol. Catal. A Chem.* 337 (2011) 68–76.
- [16] T. Arai, S. Nobukuni, A.S.D. Sandanayaka, O. Ito, Zinc porphyrins covalently bonded to the side walls of single-walled carbon nanotubes via flexible bonds: photoinduced electron transfer in polar solvent, *J. Phys. Chem. C* 113 (2009) 14493.
- [17] M. Sciarretta, M. Barawi, C. Navío, V.A.P. O’Shea, M. Blanco, J. Alemán, A graphene acid - TiO₂ nanohybrid as multifunctional heterogeneous photocatalyst for the synthesis of 1,3,4-oxadiazoles, *ACS Appl. Mater. Interfaces* 14 (2022) 34975–34984.
- [18] J.L. Nova-Fernández, D. González-Muñoz, G. Pascual-Coca, M. Cattelan, S. Agnoli, R. Pérez-Ruiz, J. Alemán, S. Cabrera, M. Blanco, Enhancing the photocatalytic activity via direct covalent functionalization in single-walled carbon nanotubes, *Adv. Funct. Mater.* 34 (2024) 2313102, <https://doi.org/10.1002/adfm.202313102>.
- [19] M. Blanco, S. Cembellín, S. Agnoli, J. Alemán, Ruthenium-p-cymene complex side-wall covalently bonded to carbon nanotubes as efficient hybrid transfer hydrogenation catalyst, *ChemCatChem* 13 (2021) 5156–5165.
- [20] D. González-Muñoz, A. Martín-Somer, K. Strobl, P.J. De Pablo, S. Diaz-Tendero, M. Blanco, J. Alemán, Enhancing visible-light photocatalysis via endohedral functionalization of single-walled carbon nanotubes with organic dyes, *ACS Appl. Mater. Interfaces* 13 (2021) 24877–24886.
- [21] M.R. Nabil, Y. Bide, S.J.T. Rezaei, Pd nanoparticles immobilized on PAMAM-grafted MWCNTs hybrid materials as new recyclable catalyst for Mizoraki-Heck cross-coupling reactions, *Appl. Catal. A* 406 (2011) 124–132.
- [22] K. Woan, G. Pyrgiotakis, W. Sigmund, Photocatalytic carbon-nanotube-TiO₂ composites, *Adv. Mater.* 21 (2009) 2233–2239.
- [23] D. Mosconi, M. Blanco, T. Gatti, L. Calvillo, M. Otyepka, A. Bakandritsos, E. Menna, S. Agnoli, G. Granozzi, Arene C-H insertion catalyzed by ferrocene covalently heterogenized on graphene acid, *Carbon* 143 (2019) 318–328.
- [24] C.-A. Wang, Y.-F. Han, K. Nie, Y.-W. Li, Porous organic frameworks with mesopores and [Ru(bpy)₃]²⁺ ligand built-in as a highly efficient visible-light heterogeneous photocatalyst, *Mater. Chem. Front.* 3 (2019) 1909–1917.
- [25] I.-H. Choi, S. Yoon, S. Huh, S.-J. Kim, Y. Kim, Photophysical properties and heterogeneous photoredox catalytic activities of Ru(bpy)₃³⁺@InBTB metal-organic framework (MOF), *Chem. Eur. J.* 26 (2020) 14580–14584.
- [26] Y.-X. Tan, S.-X. Lin, C. Liu, Y. Huang, M. Zhou, Q. Kang, D. Yuan, M. Hong, Boosting photocatalytic cross-dehydrogenative coupling reaction by incorporating [RuII(bpy)₃] into a radical metal-organic framework, *Appl. Catal. B* 227 (2018) 425–432.
- [27] M. Malizia, S.A. Scott, L. Torrente-Murciano, A.M. Boies, T.A. Aljohani, H. G. Baldovi, Enhanced visible light-driven photocatalytic water-splitting reaction of titanate nanotubes sensitized with Ru(II) bipyridyl complex, *Nanomaterials* 13 (2023) 2959.
- [28] M. Jiang, Y. Gao, Z. Wang, Z. Ding, Photocatalytic CO₂ reduction promoted by a CuCo₂O₄ cocatalyst with homogeneous and heterogeneous light harvesters, *Appl. Catal. B* 198 (2019) 180–188.
- [29] S. Jiang, J. Liu, K. Zhao, D. Cui, P. Liu, H. Yin, M. Al-Mamun, S.E. Lowe, W. Zhang, Y.L. Zhong, J. Chen, Y. Wang, D. Wang, H. Zhao, Ru(bpy)₃³⁺-sensitized 001 facets LiCoO₂ nanosheets catalyzed CO₂ reduction reaction with 100% carbonaceous products, *Nanores.* 15 (2022) 1061–1068.
- [30] A. Jana, J. Mondal, P. Borah, S. Mondal, A. Bhaumik, Y. Zhao, Ruthenium bipyridyl tethered porous organosilica: a versatile, durable and reusable heterogeneous photocatalyst, *Chem. Commun.* 51 (2015) 10746–10749.
- [31] J. Wang, S. Zhou, B. Li, X. Liu, H. Chen, H. Wang, Improving the photostability of [Ru(bpy)₃]²⁺ by embedment in silica, *ChemPhotoChem* 6 (2022) e202200124.
- [32] J.-T. Cao, Y.-L. Wang, J.-J. Zhang, Y.-X. Dong, F.-R. Liu, S.-W. Ren, Y.-M. Liu, Immuno-Electrochemiluminescent Imaging of a Single Cell Based on Functional Nanopores of Heterogeneous Ru(bpy)₃³⁺@SiO₂/Au Nanoparticles, *Anal. Chem.* 90 (2018) 10334–10339, <https://doi.org/10.1021/acs.analchem.8b02141>.
- [33] J.-M. Zen, S.-L. Liou, A.S. Kumar, M.-S. Hsia, An efficient and selective photocatalytic system for the oxidation of sulfides to sulfoxides, *Angew. Chem. Int. Ed.* 42 (2003) 577–579.
- [34] X. Li, Z. Hao, F. Zhang, H. Li, Reduced graphene oxide-immobilized tris(bipyridine) ruthenium(II) complex for efficient visible-light-driven reductive dehalogenation reaction, *ACS Appl. Mater. Interfaces* 8 (2016) 12141–12148.
- [35] S.-N. Ding, D. Shan, S. Cosnier, A. Le Goff, Single-walled carbon nanotubes noncovalently functionalized by ruthenium(II) complex tagged with pyrene: electrochemical and electrogenerated chemiluminescence properties, *Chem. Eur. J.* 18 (2012) 11564–11568.
- [36] M.A. Valle-Amores, M. Blanco, S. Agnoli, A. Fraile, J. Alemán, Oxidized multiwalled nanotubes as efficient carbocatalyst for the general synthesis of azines, *J. Catal.* 406 (2022) 174–183.
- [37] M. Amiri, G. Shul, N. Donzel, D. Bélanger, Aqueous electrochemical energy storage system based on phenanthroline- and anthraquinone-modified carbon electrodes, *Electrochimica Acta* 390 (2021) 138862.
- [38] Y. Que, J. Ruan, Y. Xiao, C. Feng, G. Lu, X. Huang, Fluorinated vesicles embedded with Ru-based catalysts as efficient and recyclable nanoreactors for photo-mediated aerobic oxidation, *Polym. Chem.* 11 (2020) 1727–1734.
- [39] D. González-Muñoz, J. Alemán, M. Blanco, S. Cabrera, Single walled carbon nanotubes with encapsulated Pt (II) photocatalyst for the oxidation of sulfides in water, *J. Catal.* 413 (2022) 274–283.
- [40] W. Huang, T. Ogawa, Spontaneous resolution of Δ and Λ enantiomeric pair of [Ru(phen)(bpy)2](PF₆)₂ (phen = 1,10-phenanthroline, bpy = 2,2′-bipyridine) by conglomerate crystallization, *Polyhedron* 25 (2006) 1379–1385.
- [41] D. Bahari, B. Babamiri, A. Salimi, R. Hallaj, S.M. Amininasab, A self-enhanced ECL-RET immunosensor for the detection of CA19-9 antigen based on Ru(bpy)₃²⁺(phen)₂²⁺ - Amine-rich nitrogen-doped carbon nanodots as probe and graphene oxide grafted hyperbranched aromatic polyamide as platform, *Anal. Chim. Acta* 1132 (2020) 55–65.
- [42] V.J. González, C. Martín-Alberca, G. Montalvo, C. García-Ruiz, J. Baselga, M. Terrones, O. Martín, Carbon nanotube-Cu hybrids enhanced catalytic activity in aqueous media, *Carbon* 78 (2014) 10–18.
- [43] M.S. Dresselhaus, G. Dresselhaus, A. Jorio, A.G. Souza Filho, M.A. Pimenta, R. Saito, Single nanotube Raman spectroscopy, *Acc. Chem. Res.* 35 (2002) 1070–1078.
- [44] J.-Y. Mevellec, C. Bergeret, J. Cousseau, J.-P. Buisson, C.P. Ewels, S. Lefrant, Tuning the Raman resonance behavior of single-walled carbon nanotubes via covalent functionalization, *J. Am. Chem. Soc.* 133 (2011) 16938–16946.

- [45] E.L. Sciuto, M.F. Santangelo, G. Villaggio, F. Sinatra, C. Bongiorno, G. Nicotra, S. Libertino, Photo-physical characterization of fluorophore Ru(bpy)₃2+ for optical biosensing applications, *Sensing and Bio-Sensing Research* 6 (2015) 67–71.
- [46] M.-E. Moret, I. Tavernelli, U. Rothlisberger, Combined QM/MM and classical molecular dynamics study of [Ru(bpy)₃]²⁺ in Water, *J. Phys. Chem. C* 113 (2009) 7737–7744.
- [47] F. Li, Z. Yang, H. Weng, G. Chen, M. Lin, C. Zhao, High efficient separation of U(VI) and Th(IV) from rare earth elements in strong acidic solution by selective sorption on phenanthroline diamide functionalized graphene oxide, *Chem. Eng. J.* 332 (2018) 340–350.
- [48] D.J. Morgan, Resolving ruthenium: XPS studies of common ruthenium materials, *Surf. Interface Anal.* 47 (2015) 1072–1079.
- [49] K. Kalyanasundaram, Photophysics, photochemistry and solar energy conversion with tris(bipyridyl)ruthenium(II) and its analogues, *Coord. Chem. Rev.* 46 (1982) 159–244.
- [50] A.G. Ryabenko, T.V. Dorofeeva, G.I. Zvereva, UV–VIS–NIR spectroscopy study of sensitivity of single-wall carbon nanotubes to chemical processing and Van-der-Waals SWNT/SWNT interaction. Verification of the SWNT Content Measurements by Absorption Spectroscopy, *Carbon* 42 (2004) 1523–1535.
- [51] M. Müller, R. Meinke, J. Maultzsch, Z. Syrgiannis, F. Hauke, Á. Pekker, K. Kamarás, A. Hirsch, C. Thomsen, Electronic properties of propylamine-functionalized single-walled carbon nanotubes, *ChemPhysChem* 11 (2010) 2444–2448.
- [52] S.M. Bonesi, I. Manet, M. Freccero, M. Fagnoni, A. Albini, Photosensitized oxidation of sulfides, *Chem. Eur. J.* 12 (2006) 4844–4857.
- [53] M. Okamoto, Temperature dependence of the nearly diffusion-controlled fluorescence quenching by oxygen of 9,10-dimethylantracene in liquid solution, *Phys. Chem. Chem. Phys.* 3 (2001) 3696–3700.
- [54] A. Casado-Sánchez, M. Uygur, D. González-Muñoz, F. Aguilar-Galindo, J.L. Nova-Fernández, J. Arranz-Plaza, S. Diaz-Tendero, S. Cabrera, O. García Mancheno, J. Alemán, 8-mercaptoquinoline as a ligand for enhancing the photocatalytic activity of Pt (II) Coordination complexes: reactions and mechanistic insights, *J. Org. Chem.* 84 (2019) 6437–6447.
- [55] S. Anselmi, S. Liu, S.-H. Kim, S.M. Barry, T.S. Moody, D. Castagnolo, A mild and chemoselective CALB biocatalysed synthesis of sulfoxides exploiting the dual role of AcOEt as solvent and reagent, *Org. Biomol. Chem.* 19 (2021) 156–161.
- [56] S. Gan, J. Yin, Y. Yao, Y. Liu, D. Chang, D. Zhu, L. Shi, Metal- and additive-free oxygen-atom transfer reaction: an efficient and chemoselective oxidation of sulfides to sulfoxides with cyclic diacyl peroxides, *Org. Biomol. Chem.* 15 (2017) 2647–2654.